Supporting information

3D printable, super compressible, antibacterial and environmentally stable dual networked ionogels as wearable pressure sensors for wireless early warning of precise health

Xiaoya Liu[a], Zhenzhou Wang[b], Haoyu Wang[b], Yuqi Liu[b], Zhice Xu[a], Shaorui Chen[a*], Xudong Yu[a*]

[a] *Hebei Provincial Key Laboratory of Photoelectric Control on Surface and Interface, and College of Science, Hebei University of Science and Technology, Yuxiang Street 26, Shijiazhuang 050080, PR China*

[b] *School of Information Science and Engeering, Hebei University of Science and Technology, Yuxiang Street 26, Shijiazhuang 050080, PR China*

* Corresponding author

* *E-mail address*: sjz_wgq@126.com (S. Chen), chemyxd@163.com (X. Yu)

S1. Experimental section

S1.1 characterizations

The microstructure of the gel was observed by Quattro S field emission scanning electron microscope (ESEM). Fourier-transform infrared spectroscopy (Hench LIDA-20 FTIR) was used to determine the chemical structure of the gel, with a range of 400-4000 cm^{-1}, a resolution of 4 cm^{-1}, and 16 scans. Thermogravimetric analysis (TGA) was performed on a SDT 2960 thermogravimetric analyzer under nitrogen or air atmospheres from 30 to 800 ° C with heating rates of 10 ° C min-1. Differential scanning calorimetry (DSC) was performed on a DSC 200F3 analyzer under nitrogen atmosphere from -150 to 50 ° C with heating rates of 5 ° C min^{-1}. The rheological measurements were recorded on an Anton Paar MCR 720e rheometer using a CP20-1 cone plate tool. Each sample was placed between the shear plates of the rheometer, and its strain, sweep frequency and other rheological properties were recorded at 25 °C. The stress-strain curve was tested by LD24.202 universal testing machine with a tensile rate of 50 mm min^{-1}, and the compression curve was tested by C610 universal testing machine with a compression rate of 5 mm min-1. All electrochemical characterizations were performed by CHIT60E electrochemical workstation, including EIS, LSV, IT and other electrochemical tests. The conductivity of the gel sample could be calculated by $\sigma = L / (R \times S)$, where L corresponds to the distance between the electrodes, S denotes the cross-sectional area of the sample, and R the bulk resistance measured by the multimeter. The compression sensitivity could be calculated by $S = \triangle I / (I_0 \times \triangle P)$, $\triangle I$ was the change value of current, I_0 was the initial current, $\triangle P$ was the change value of pressure.

S1.2 Detailed test methods

Mechanical properties

The mechanical properties tests of the ionogels were performed using CMT4202GD universal testing machine (China) at room temperature. The uniaxially stretching dumbbell shape ionogels (20 mm × 4 mm× 1 mm) were used in the tensile and cyclic stretch tests. The stretch speed was 100 mm/min and the load cell was 200 N. In the loading and unloading cyclic stretching examinations, the sample strips of the ionogels were first stretched to the 200 preset strains and then unloaded to zero force both at a stretch speed of 20 mm/min. The uniaxially stretching elongated shape ionogels (30 mm × 10 mm × 1 mm) were used in the tear resistance tests. The tear energy was calculated using the following equation, $G_c = 6Wc/\sqrt{\lambda_c}$, where G_c means tear energy, c means pattern notch length, λ_c means elongation at break of notched sample plus one and W means the stress-strain integral of notch-free pattern was integrated to the energy calculated by λ_c.

In the compression test, cylindrical (10 mm diameter × 10 mm height) ionogels were compressed to a maximum strain of 97%. The loading-unloading cycles were conducted at a constant compression speed of 6 mm/min. In the loading and unloading cyclic compress examinations, the ionogels were first compressed to a preset compressive strain of 80 and then unloaded to zero force both at a compressed speed of 5 mm/min.

Ionic conductivity

Cylindrical gel samples (8 mm diameter × 2 mm height) were used to measure the conductivity property of the ionogels using electrochemical workstation (CHI760E, Shanghai, China). The ionogels was put between two parallel aluminum electrodes to form an enclosed electrical circuit. The ionic conductivity of the gel was measured by the electrochemical impedance spectroscopy (EIS) in a frequency range of 1 ~ 10^5 Hz.The volume resistance R is determined by the intercept with the real axis. The electric ionic conductivity (σ) was calculated using the following equation $\sigma = L/RS$, where L, R, and S refer to the

distance between two electrodes, the cross-sectional area, and the resistance of the gel sample, respectively. In the -0.1 ~ 0.1v voltage, the linear sweep voltammetry (LSV) was used to measure the I-V curve of ionic gel under different pressure.

Extreme environmental resilience

The ionogel samples were stored in environmental chamber (LGDX2-60+300B1, Shanghai, China) at -20 °C, 0 °C and 80 °C for 30 min, and conducted tensile tests with a mass spectrometer at a tensile speed of 100 mm·min^{-1} to study its anti-freezing properties. In addition, the sensing properties of the gel were measured at -20°C and 80°C.

Optical Property

Ionogel samples were molded into 0.5 mm thick sheets, and the UV and visible light (400-800 nm) transmission rates of the ionogels were tested using a UV-vis spectrophotometer. The transmittance of the ionogel was also visually observed through coating the gel on the photo.

Strain Sensing

For the strain sensing property, the ionogel was stretched with the strain ranging from 0-1500%. The change of resistance as the strain was measured by using resistance meter (HPS2510A, Helpass Electronic Technologies, Inc.). The Ionogel was connected to a complete circuit to collect real-time resistance data. The relative resistance is calculated by the following equation:

$$\Delta R/R_0 = (R - R_0)/R_0$$

Where R_0 refers to the initial resistance without strain, and R refers to the real-time resistance with applied strain. The gauge factor (GF) was obtained by the slope of the relative resistance change ($\Delta R/R_0$)-strain (ε) curve, and was calculated by the following equation:

$$GF = \frac{\Delta R/R_0}{\varepsilon} \times 100\%$$

Ionogel as a strain sensor was measured by connecting it to a wire and its relative resistance change was collected by using the resistance meter. Then, the gel was adhered to the author's skin for human motion detection examinations, and the joint motions and minor physiological activities were monitored by the change in resistance.

Pressure sensing

For the pressure sensing property, the ionogel was compressed with the stress ranging from 0.45 Pa-2.0 MPa. The change of current as the compressive strain was measured by using electrochemical workstation (CHI760E, Shanghai, China). A real-time current-time (I-t) curve was collected by connecting the ionogel to a complete circuit with the utilization of a constant voltage (2V). The relative current is calculated by the following equation:

$$\Delta I/I_0 = (I - I_0)/I_0$$

Where I_0 refers to the initial current without compressive strain, and I refers to the real-time current with applied compressive strain. The cylindrical ionogels (10 mm diameter × 5 mm height) were used in sensitivity tests,the compression sensitivity could be calculated by the following equation:

$$S = \Delta I / (I_0 \times \Delta P)$$

ΔI was the change value of current, I_0 was the initial current, ΔP was the change value of pressure. Then, the gel was adhered to the author's nose, pulse, finger and soles of feet for human motion detection examinations, and the respiratory pulse and various movement states were monitored by the change in current.

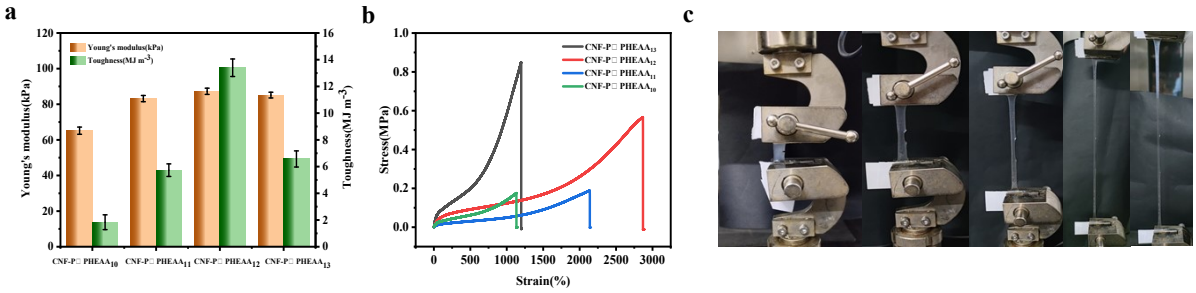

Fig. S1. a) Corresponding Young's modulus and toughness of ionogels, b) Stress-strain curves of notched ionogels (width: 10 mm, linear notch width: 2 mm), c) Photos of CNF-P@PHEAA$_{12}$ with crack during stretching.

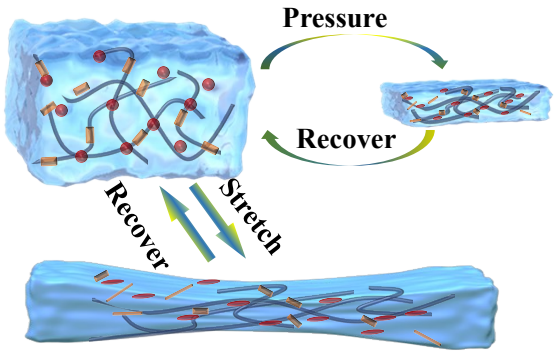

Fig. S2. A schematic representation of the destruction and reformation of ionogel physical crosslinking during the deformation.

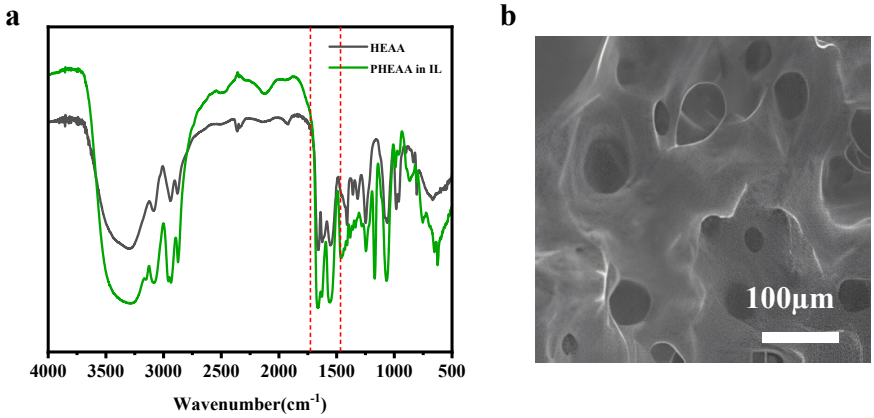

Fig. S3. a) IR Spectra of HEAA and PHEAA in [BMIM]Cl, b) Photos of ESEM

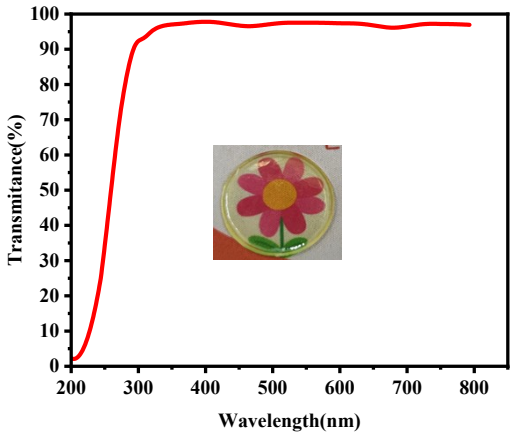

Fig. S4. Transmittance spectrum (200-800 nm) of the ionogel (thickness: 1.0 mm) with the inset photograph showing the ionogel over an image.

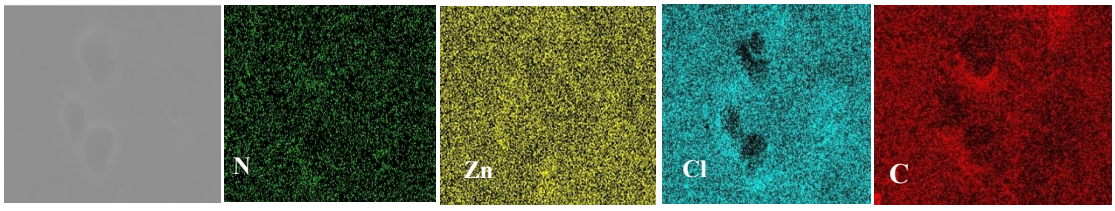

Fig. S5. EDS image of N, Zn, Cl and C in CNF-P@PHEAA$_{12}$.

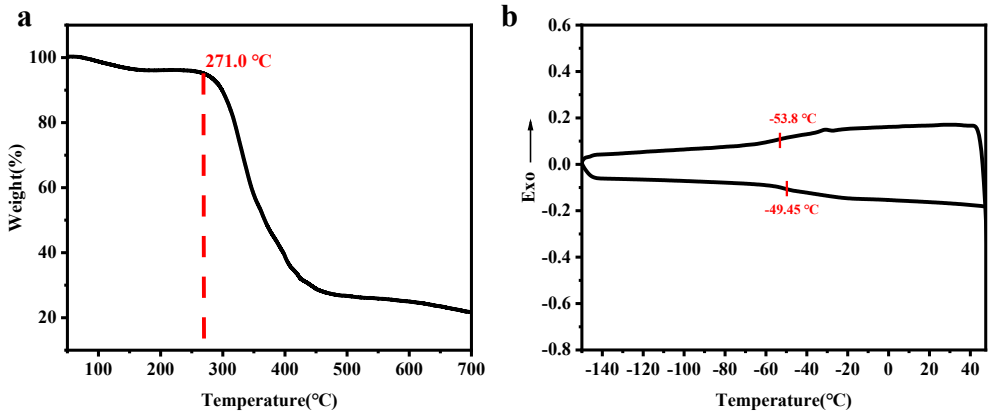

Fig. S6. a) Thermogravimetric analysis (TGA) of CNF-P@PHEAA$_{12}$ from 25 to 800 °C, heating rate: 10 °C·min^{-1}, b) Differential scanning calorimetry (DSC) plots of CNF-P@PHEAA$_{12}$ from -150 ◦C to 50 ◦C.

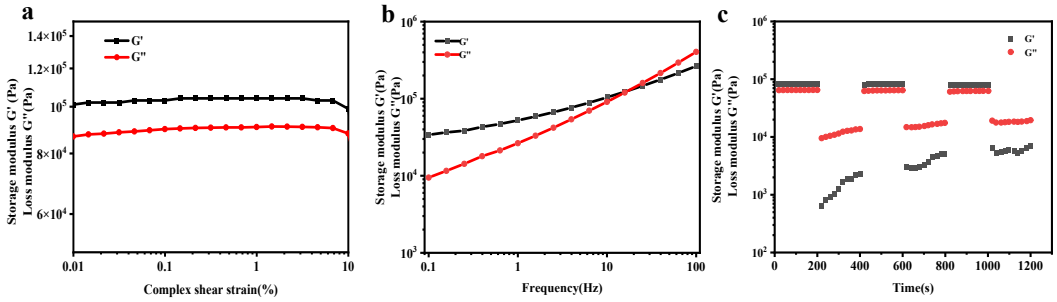

Fig. S7. Changes of storage modulus (G') and loss modulus (G") as functions of oscillation strain (a), angular frequency (b) and recovery experiment (c) at 25 ◦C for ionogel

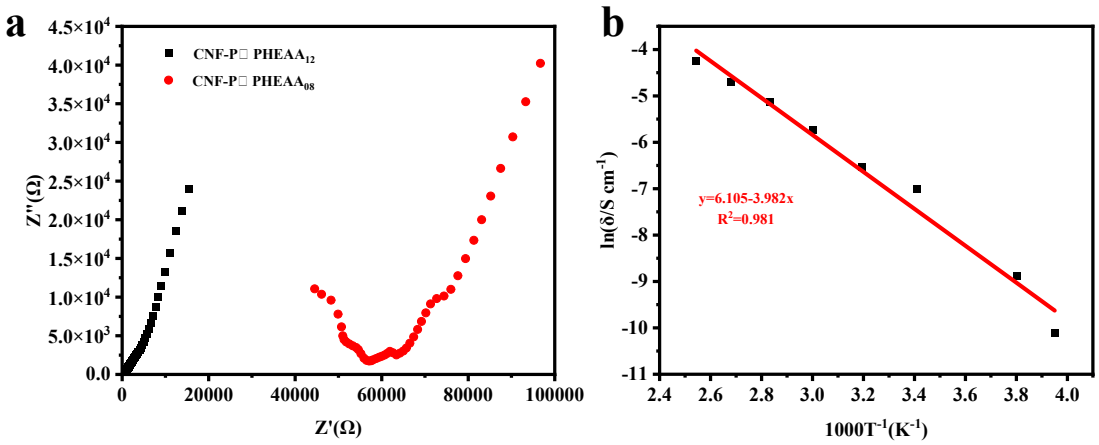

Fig. S8. a) EIS plots of CNF-P@PHEAA$_{09}$ and CNF-P@PHEAA$_{12}$, b) Arrhenius plots for ion conductivities at different temperature.

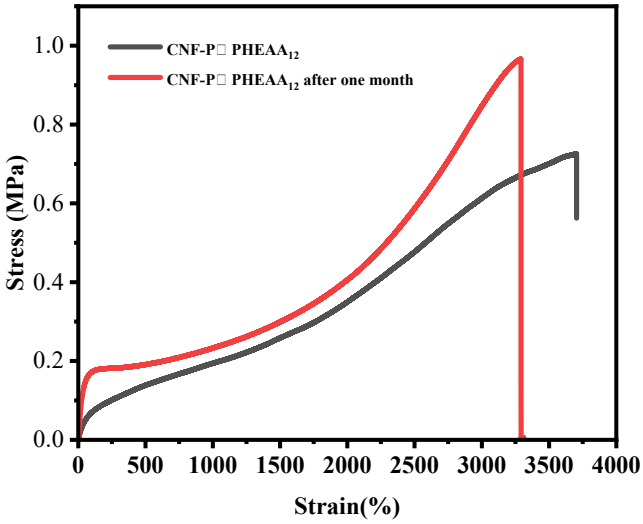

Fig. S9. Stress-strain curves of CNF-P@PHEAA$_{12}$ before and after one month

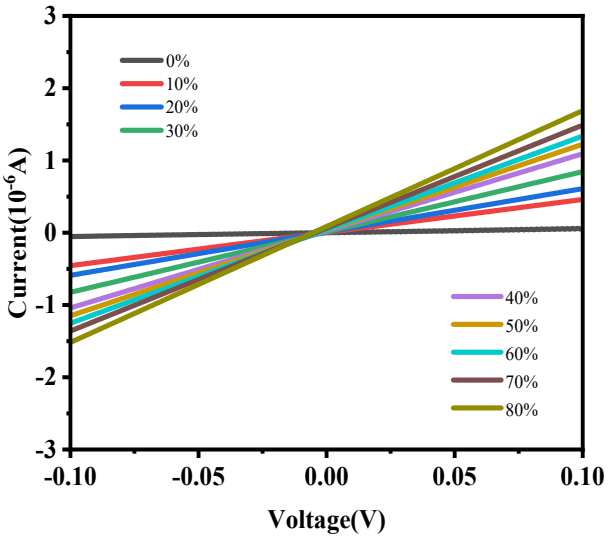

Fig. S10. Current-voltage characteristics of CNF-P@PHEAA$_{12}$ under different pressure.

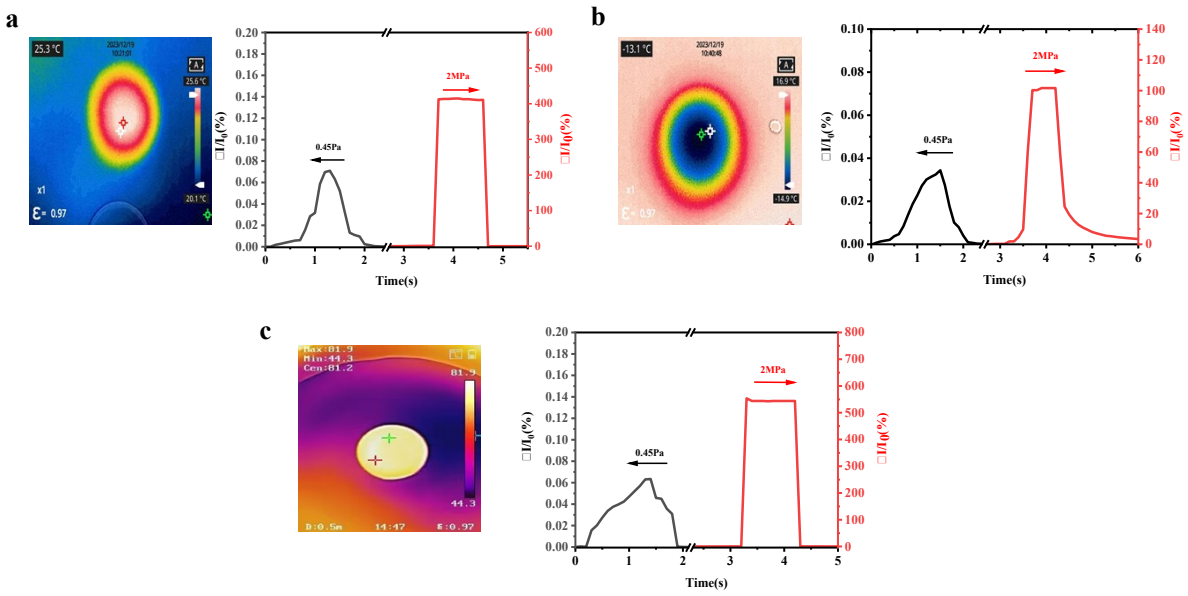

Fig. S11. a) left: Real-time infrared picture of as-prepared pressure sensors at 25°C, right: The sensing curves of tiny pressure and high pressure at 25 °C, b) left: Real-time infrared picture of as-prepared pressure sensors at -13 °C, right: The sensing curves for tiny and high pressures at -13 °C, c) left: Real-time infrared picture of as-prepared pressure sensors at 80 °C, right: The sensing curves for tiny and high pressures at 80 °C.

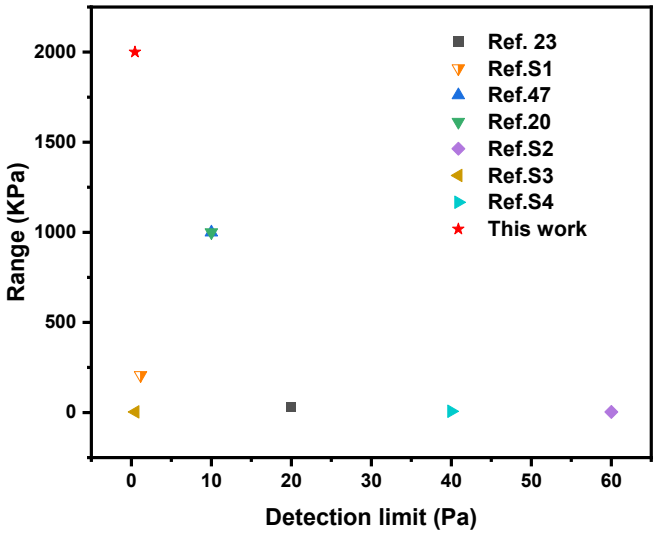

Fig. S12. Comparison of low detection limit and response range of this work with reported literatures.

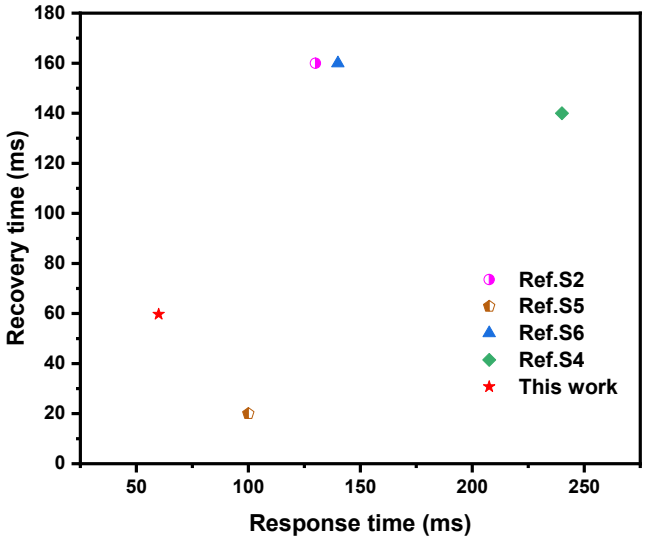

Fig. S13. Comparison of response and recovery time of this work with reported literatures.

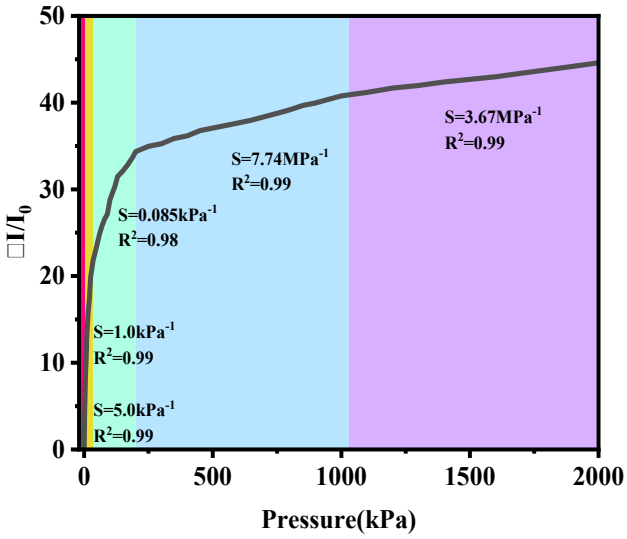

Fig. S 14. Sensitivity of the ionogel pressure sensor in the range of 0-2000 kPa.

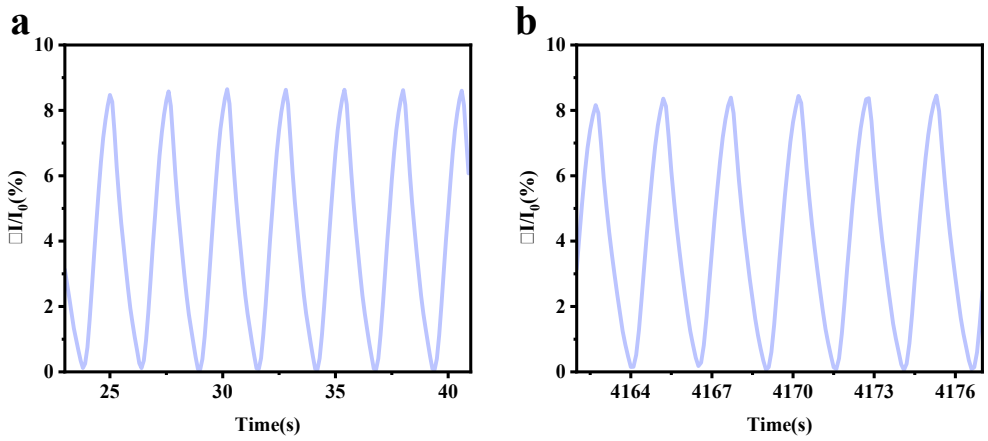

Fig. S15. A partial magnification of current change ($\Delta I/I_0$) of the sensor under 50 kPa for 1000 cycles, a) at 20-40 s, b) at 4100- 4200 s.

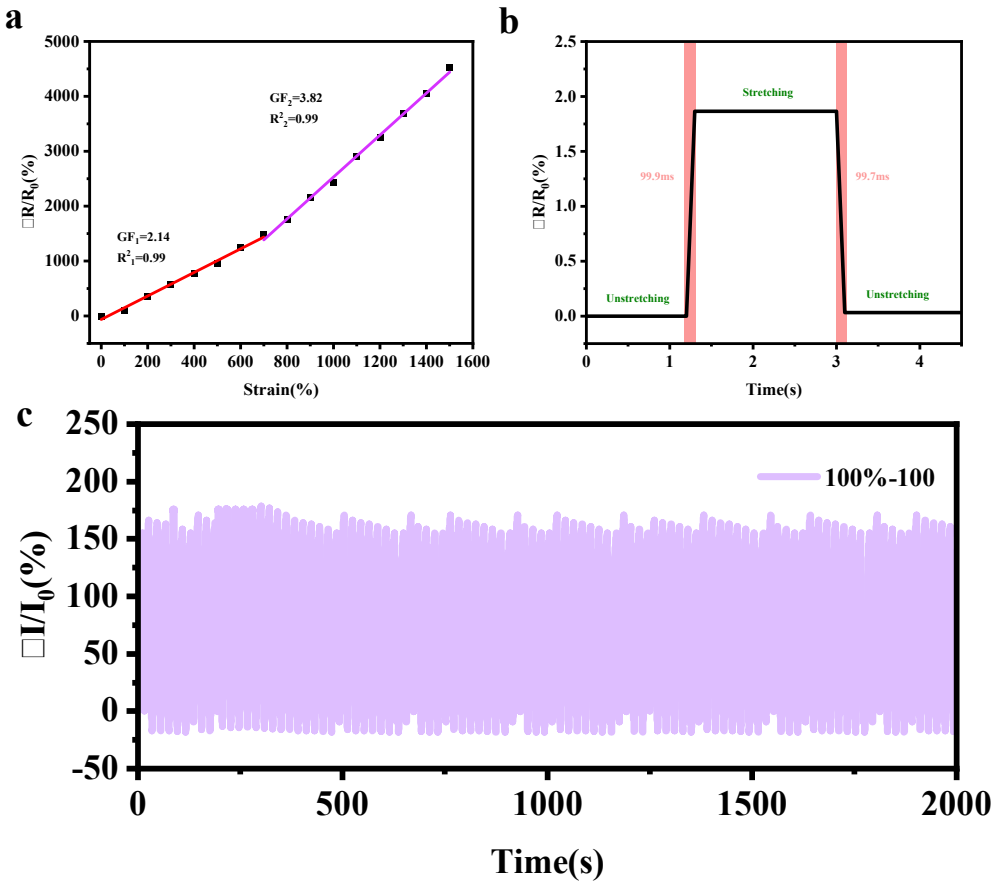

Fig. S16. a) Relative resistance changes under different strain level, b) Response time and relaxation time of ionogel sensor during loading-unloading process, c) Cyclic relative resistance of CNF-P@PHEAA$_{12}$ at strain of 100%

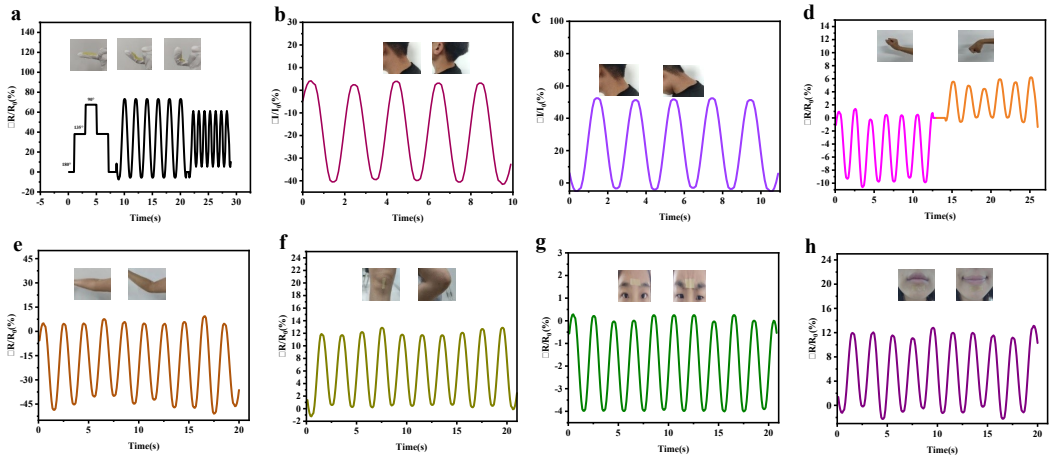

Fig. S17. Relative resistance changes of ionogel sensors for real-time detection of human motions: (a) finger bending (30 °, 60 °, 90 °), b) head down, c) head up, d) wrist bending, e) elbow bending, f) knee bending, g) frown, h) smile.

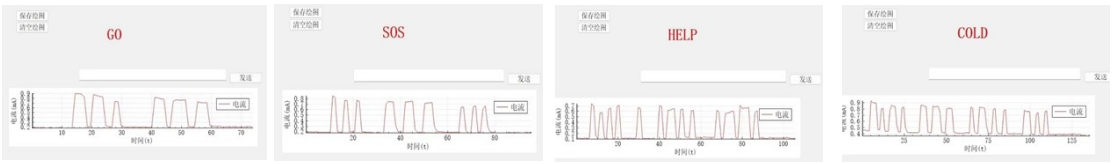

Fig. S18. The photographs of real-time transmission information through Morse code

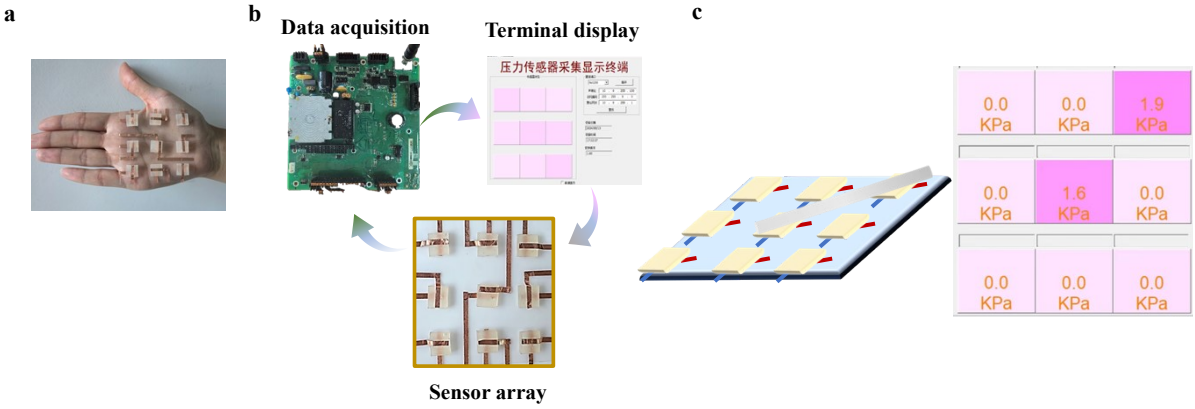

Fig. S19. Photographs(a) and schematic diagram (b) of 3 × 3 sensor array, c) the responses of the sensing array to glass rod.

Table S1 Effect of CNF-P, HEAA and IL contents of ionogels on tensile stress-strain[a]

Ionogels	CNF-P/g	HEAA/g	[BMIM]Cl/g	ultimate stress/MPa	strain/%
CNF-P@PHEAA$_{01}$	0.005	0.7	0.5	0.315	14
CNF-P@PHEAA$_{02}$	0.005	0.9	0.5	2.67	6
CNF-P@PHEAA$_{03}$	0.005	1.1	0.5	6.0	4
CNF-P@PHEAA$_{04}$	0.005	0.9	0.6	0.59	12
CNF-P@PHEAA$_{05}$	0.005	0.9	0.7	0.419	20
CNF-P@PHEAA$_{06}$	0.007	0.9	0.6	0.9	16
CNF-P@PHEAA$_{07}$	0.009	0.9	0.6	1.7	13
CNF-P@PHEAA$_{08}$	0.007	0.9	0.65	1.0	15.6

[a] UV184: 1.0 wt % with respect to HEAA

Table S2 Effect of different components of ionogels on tensile stress-strain[a]

Ionogels	$ZnCl_2$/ g	H_2O/g	CNF-P/g	HEAA /g	[BMIM]Cl/ g	ultimate stress/MPa	strain /%
CNF-P@PHEAA$_{10}$	0.15	0.2	0	0.9	0.65	0.28	12
CNF-P@PHEAA$_{11}$	0.15	0.2	0.003	0.90	0.65	0.31	34
CNF-P@PHEAA$_{12}$	0.15	0.2	0.007	0.90	0.65	0.725	37
CNF-P@PHEAA$_{13}$	0.15	0.2	0.01	0.90	0.65	1.0	15.8

[a] UV184: 1.0 wt % with respect to HEAA

Table S3 Effect of $ZnCl_2$ and H_2O contents of ionogels on stress-strain and conductive properties at 20 °C[a]

Ionogels	$ZnCl_2$/ g	H_2O/ g	CNF-P/g	HEAA/g	[BMIM]Cl/ g	ultimate stress/MPa	strain /%	conductivity /mS cm^{-1}
CNF-P@$PHEAA_{08}$	0	0	0.007	0.9	0.65	1.0	15.6	0.001
CNF-P@$PHEAA_{14}$	0.1	0.2	0.007	0.9	0.65	0.44	36	1.37
CNF-P@$PHEAA_{12}$	0.15	0.2	0.007	0.9	0.65	0.725	37	0.95
CNF-P@$PHEAA_{15}$	0.2	0.2	0.007	0.9	0.65	1.1	8	0.65
CNF-P@$PHEAA_{16}$	0.15	0.15	0.007	0.9	0.65	1.1	15	0.4
CNF-P@$PHEAA_{17}$	0.15	0.25	0.007	0.9	0.65	0.33	32	1.2

[a] UV184: 1.0 wt % with respect to HEAA

Table S4 Comparison of relevant information of pressure sensor with other literatures[a]

Materials	Detection limit	Max. press-ure	3D printing	Sensitivity	A.P.[b]	Overall performance	Ref.
CNF-P@PHEAA$_{12}$	0.45Pa	2MPa	✓	0-0.13kPa: 5.0 kPa^{-1} 0.13-1kPa: 1.9 kPa^{-1}	✓	antibacterial properties, 3D printing, broad response range, low detection limit, high sensitivity	This Work
1-[BMIM][BF$_4$] PIL ionogels	10Pa	1MPa	-	0-0.51 kPa: 0.04 kPa^{-1}	✓	antibacterial properties, wide response range, low sensitivity	Ref. 48
PIL/XG ionogel	-	100 kPa	-	0-2 kPa: 0.24 kPa^{-1} 2-8 kPa: 0.02 kPa^{-1} 8-100kPa: 1.24×10^{-3} kPa^{-1}	✓	antibacterial properties, narrow response range, low sensitivity	Ref. 21
AAm/TEFA ionogel	10Pa	1MPa	-	0-10 kPa: 0.81 kPa^{-1}	-	wide response range, high detection limit, low sensitivity	Ref. 20
PUA/ACMO ionogel	-	2.05 kPa	✓	0-0.5 kPa: 0.717 kPa^{-1}	-	3D printing, narrow response range, low sensitivity,	Ref. 1
$Ti_3C_2T_x$-MXene	7.2Pa	2MPa	-	7.2-2MPa: 0.14-0.87 kPa^{-1}	-	narrow response range, low sensitivity,	Ref. 49
MRDN hydrogel	600Pa	1.2 MPa	✓	0-5kPa: 0.018 kPa^{-1}	-	3D printing, wide response range, low sensitivity	Ref. 50

[a] “-” means no detection or no reported.

[b] Antibacterial properties

References

[S1] J. Chen, G. Zhu, J. Wang, X. Chang, Y. Zhu, *ACS Appl. Mater. Interfaces*, 2023, **15**, 7485-7495.

[S2] D. Liao, Y. Wang, P. Xie, C. Zhang, M. Li, H. Liu, L. Zhou, C. Wei, C. Yu, Y. Chen, *J. Colloid. Interf. Sci.*, 2022, **628**, 574-587.

[S3] H. Cheng, B. Wang, K. Yang, C. Wang, *J. Mater. Chem. C*, 2021, **9**, 1014-1024.

[S4] Y. Zou, Z. Chen, X. Guo, Z. Peng, C. Yu, W. Zhong, *ACS Appl. Mater. Interfaces*, 2022, **14**, 17858-17868.

[S5] Y. Lv, J. Wei, Z. Huang, Z. Zhang, S. Ding, C. Zhang, W. Wang, K. Xu, R. Xu, L. Wang, Y. Guo, Y. Chen, *Chem. Eng. J.*, 2024, **488**, 151053.

[S6] X. Zhang, S. Liu, X. Wang, J. Peng, W. Yang, Y. Ma, K. Fan, *J. Colloid. Interf. Sci.*, 2024, **654**, 1348-1355.